Reliability Engineering and System Safety 245 (2024) 109974

Contents lists available at ScienceDirect

Reliability Engineering and System Safety

journal homepage: www.elsevier.com/locate/ress

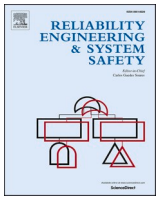

A neural network approach to predict the time-to-failure of atmospheric tanks exposed to external fire

Nicola Tamascelli [a,b], Giordano Emrys Scarponi [a], Md Tanjin Amin [c], Zaman Sajid [c], Nicola Paltrinieri [b], Faisal Khan [c], Valerio Cozzani [a,*]

[a] LISES – Laboratory of Industrial Safety and Environmental Sustainability, DICAM - Department of Civil, Chemical, Environmental and Materials Engineering, University of Bologna, via Terracini n.28, 40131 Bologna, Italy
[b] Department of Mechanical and Industrial Engineering, NTNU, Trondheim, Norway
[c] Mary Kay O'Connor Process Safety Center, Artie McFerrin Department of Chemical Engineering, Texas A&M University, College Station, TX 77843-3122, USA

ARTICLE INFO

Keywords:
Domino effect
Time-to-failure
Escalation
Cascading events
Fire
Artificial intelligence
Neural networks

ABSTRACT

Domino scenarios triggered by fire pose severe risks to workers, assets, and the environment. Accurate quantitative models are needed to support mitigation actions addressing the prevention of fire escalation, especially considering sensitive targets such as atmospheric tanks containing large quantities of dangerous substances. A novel approach based on neural networks was developed, allowing the accurate quantification of the time-to-failure (TTF) of atmospheric tanks exposed to external fires accounting for mitigation actions. Data from a lumped parameter model were used to train and assess neural networks' performance. The toolbox of models obtained provides the TTF of atmospheric tanks both in the case of unmitigated fire scenarios and considering safety barriers and protection measures, such as water deluges and fire monitors. Model predictions are fast, accurate, and supplemented with confidence intervals. The comparative analysis demonstrated the better performance of the model developed compared to simplified correlations widely used in the literature to predict TTF. The approach developed, based on the integration of neural networks in consequence analysis tools, shows significant potential for the advancement of a quantitative assessment of domino scenarios, providing accurate and user-friendly tools for a quick evaluation of domino fire scenarios under both mitigated and unmitigated conditions.

1. Introduction

Fires are the most frequent type of accident in chemical facilities [1]. Fire scenarios have inherent characteristics that can jeopardize the safety of workers and nearby residents while also causing severe economic losses [2]. In addition, fire scenarios are a frequent cause of domino effects, triggering cascading events escalating into more severe accidents. Some of the most severe accidents in the last two decades indicate that fires play a leading role in domino scenarios [3,4]. Remarkable examples are the accident that occurred in 2007 at the Valero refinery in Sunray, Texas, accounting for approximately $50 million in property damage and four injuries [5], the fires and explosions that occurred in 2009 in Jaipur, India, causing 13 deaths and more than 200 injuries [6], and the accident that took place in 2019 in Houston, USA, where 14 naphtha tanks burned for three days causing property damage exceeding $150 million [7]. Domino scenarios are described as low-probability high-impact (HILP) events and involve chains of events triggered by an initial incident, leading to a cascading effect with potentially severe consequences and elevating the potential for major accidents [8,9]. The risk of domino effects escalates as chemical plants become more concentrated and densely packed, emphasizing the critical importance of proactive safety measures and risk assessments to prevent such cascading incidents [10,11].

Flammable substances are often stored in large atmospheric tanks [2], which may contain up to 80000 m^3 of hazardous liquids. Domino scenarios involving storage tanks are considered particularly critical due to the quantity of the substance involved and the spatial vicinity between tanks in storage facilities. For this reason, it is vital to evaluate the response of atmospheric tanks when a fire occurs in their proximity.

When exposed to thermal loads, the tank shell is expected to undergo substantial deformation caused by thermal stresses and internal pressure build-up, which can lead to failure [12,13]. For these reasons, passive (e.

* Corresponding author.
E-mail address: valerio.cozzani@unibo.it (V. Cozzani).

https://doi.org/10.1016/j.ress.2024.109974
Received 11 September 2023; Received in revised form 30 December 2023; Accepted 26 January 2024
Available online 28 January 2024

g., thermal insulation) and active devices (e.g., fixed water or foam sprays and water deluge systems) that mitigate the effect of the fire [14] are frequently implemented. The time between the start of the fire and the possible failure of the tank, namely the time-to-failure (TTF), is thus influenced by the design features of the tank (e.g., diameter, height, and shell thickness), by operating parameters (e.g., filling degree, substance density, and vapor pressure), by the fire scenario (e.g., thermal radiation and view factor), and by the performance of passive and active safety systems installed.

The quantification of the TTF is critical for estimating the probability of failure and, eventually, for quantifying the risk associated with escalation resulting in domino scenarios. Hence, there is a compelling need to issue methods for the quantification of the TTF of atmospheric tanks considering (i) fire characteristics, (ii) tank characteristics, and (iii) safety barriers. Rigorous modelling through coupled computational fluid dynamics (CFD) and finite element modelling (FEM) can be used to evaluate the structural response of tanks exposed to external fire [15]. For example, Iannaccone et al. [16] and Scarponi et al. [17] used CFD modelling to simulate the pressure and temperature profiles of LNG and LPG pressurized tanks. Masum Jujuly et al. [18] simulated the effect of a pool fire caused by LNG spill on multiple targets. A model for the dynamic evaluation of the fire response of steel storage tanks integrating CFD and FEM analysis was presented by [19]. Similar approaches were proposed by Wang et al. [20] and Jianfeng Yang et al. [21]. However, the expertise in setting up the simulations and the substantial computational resources required to run them hinder their widespread application. In current practice, CFD and FEM simulations need substantial data, and model validation is challenging and time-consuming within risk assessment studies. When considered, it is usually applied only for the deterministic analysis of single critical scenarios. To overcome this issue, Gubinelli [22] proposed a lumped model called RADMOD to estimate the TTF of atmospheric tanks exposed to external fires.

The limited computational resources required to run RADMOD simulations result in a significant reduction of simulation time than in FEM simulations. However, the computational time required still makes this approach not suitable for advanced applications, such as dynamic risk analysis [23,24] and dynamic probabilistic risk assessment [25], which often require the simulation of a large number of scenarios for the quantification of accident paths. To overcome this limitation, Landucci et al. [26] used the results of RADMOD simulations to develop a simplified analytical correlation that explicitly correlates the dependency of the TTF on the heat load and tank volume. Recently, Yang et al. [27] proposed an improved correlation where parameters were fitted on results from CFD and FEM simulations.

To the best of the authors' knowledge, the methodologies proposed by Landucci et al. [26] and Yang et al. [27] are the only methods currently available capable of rapidly estimating the TTF of tanks exposed to external fire. Requiring limited computational resources is crucial for model integration into frameworks for the dynamic risk analysis of fire-induced scenarios – as those proposed, e.g., by [28–33] – which all rely on the abovementioned correlations for the estimation of the TTF. However, notwithstanding the popularity of the approach proposed by Landucci et al. [26], the following limitations must be acknowledged [34–36]:

- The correlations above were derived from limited datasets based on a predefined set of tank geometries, which could restrict their generalization capabilities;
- The error in the TTF with respect to the original dataset values is relatively high, especially considering scenarios with large TTFs;
- They do not provide the confidence level of predictions;
- They tend to produce over-conservative results;
- Only a single study attempted to incorporate the influence of safety barriers into the simplified correlations for the TTF [37], still suffering from the limitations listed above.

In this context, Artificial Intelligence (AI) and Machine Learning (ML) present intriguing opportunities to address some of the limitations mentioned above. In fact, advanced ML algorithms can learn directly from failure data to develop predictive models that balance accuracy with the use of computational results and the time required to run simulations. In the framework of safety and reliability, the application of ML is a relatively new yet promising area of research [38]. Recent studies have seen a surge in research on fault detection and diagnosis [39,40], anomaly detection [41,42], system prognosis [43,44], reliability analysis [45,46], and risk analysis [47]. In particular, when considering system prognosis, numerous studies have proposed the use of ML to estimate the Remaining Useful Life (RUL) of degrading equipment, including lithium batteries [48], bearings (J. [49]), induction motors [43], turbofans [50], wind turbines [51].

However, a significant gap is still present in the literature concerning the application of ML for the prediction of the impact of fires on atmospheric tanks. Actually, recent studies have explored the use of ML techniques to develop surrogate models based on data from Computational Fluid Dynamics (CFD) and Finite Element Method (FEM) simulations [52,53]. For instance, Li et al. [54] applied a graph neural network to predict the overpressure resulting from simulated Boiling Liquid Expanding Vapor Explosions (BLEVE). Similarly, Ye and Hsu [55] used CFD and FEM data to model 1200 fire scenarios in a steel roof structure with fixed geometry and then employed this data to train a Long Short-Term Memory (LSTM) Neural Network to predict structural displacement. However, to the best of the authors' knowledge, there is a notable lack of research specifically targeting the estimation of the TTF of atmospheric tanks exposed to external fires using ML. Only one recent contribution, concurrent with our research, proposes a ML-based method to estimate the structural integrity of tanks under fire conditions [56]. Yet, this method primarily focuses on calculating failure probability rather than directly estimating TTF, and does not consider the effect of mitigation barriers.

The present study has developed a novel approach to bridge the aforementioned gaps. Neural networks (NN) were used to quantify the TTF of atmospheric tanks exposed to external fires. Simulated data from the RADMOD model were used to build an extensive dataset containing 4896 scenarios with different tank geometries and fire characteristics. The influence of safety barriers and safety systems is included in the model, considering a comprehensive set of protection measures characterized by various activation times and effectiveness. A model toolbox was obtained, allowing the estimation of the TTF of both unmitigated scenarios and considering the effect of different protection measures. Hyperparameters fine-tuning was performed to ensure optimal performance and good generalization capabilities.

Furthermore, to enhance the model output and account for prediction uncertainties, a model-agnostic approach was applied to estimate confidence intervals. By this approach, the model returns a single-point prediction for the TTF and a range of values with a specified confidence level. This comprehensive output captures the inherent uncertainty in the data and the model, providing a more informative and robust assessment. The novel contributions of this study can be summarized as follows:

- the proposed NN-based toolbox represents an innovative, user-friendly, and computationally inexpensive approach for the estimation of the TTF of atmospheric tanks exposed to external fires;
- the approach allows for the explicit modelling of the impact of safety barriers, enabling a detailed and accurate analysis of their effectiveness in various scenarios;
- the use of a comprehensive dataset encompassing various tank geometries, fire characteristics, and barrier configurations improves model robustness and generalizability;
- confidence intervals are provided to enhance model interpretability, robustness, and credibility.

A comparative analysis between the models developed in this study and the simplified correlations proposed by Landucci et al. [26] and Yang et al. [27] shows that the new models have a better performance.

The paper is organized into five sections, including this introductory paragraph. Section 2 outlines the methodology, addressing data generation and preprocessing, developing the NN models and their evaluation, fine-tuning hyperparameters, and generating confidence intervals. Section 0 presents the results, showcasing the performance obtained by the models and providing a comparative analysis with similar approaches found in the literature. Results are discussed in Section 4, and conclusions are drawn in Section 5. The models developed are included in the Supplementary materials and are freely available for use by researchers ("TTF_unmitigated.dill" and "TTF_mitigated.dill", "TTF_deluge.dill"). Also, a quick guide ("Model Configuration and Usage.pdf") is provided to prepare a Python environment for importing and using the models.

2. Methodology

The methodology used to build the NN models is schematized in Fig. 1. First, a lumped parameter model known as RADMOD [22] was used to create two datasets (step 1 in Fig. 1): one containing failure data related to unmitigated fire scenarios ($\mathscr{D}$) and the other incorporating the effect of protective measures ($\overline{\mathscr{D}}$). These datasets were then preprocessed and split into two parts (step 2 in Fig. 1). The first part (i.e., $\mathscr{D}_{train}$ and $\overline{\mathscr{D}}_{train}$ in Fig. 1) was used to train the models, while the second part (i.e., $\mathscr{D}_{eval}$ and $\overline{\mathscr{D}}_{eval}$ in Fig. 1) was used to evaluate their prediction performance. Subsequently, the models' hyperparameters were fine-tuned through a grid-search procedure to ensure optimal performance (step 5 in Fig. 1). The resulting optimized models, namely $\mathscr{M}^*$ and $\overline{\mathscr{M}^*}$, can be utilized to predict the TTF of unmitigated and mitigated fire scenarios. In addition, a reference version of the model $\overline{\mathscr{M}^*}$ is offered to account for the influence of a standard generic water deluge system, useful in preliminary screening activities (step 6 in Fig. 1). Finally, a procedure for estimating confidence intervals was implemented to provide more informed judgments based on the confidence level associated with the predictions (step 7 in Fig. 1). A detailed description of each step of the methodology is provided in the following.

2.1. Simulated failure data

Two series of simulations were carried out to generate failure data for different atmospheric tanks subject to various fire conditions. The first set of simulations focused on unmitigated scenarios, while the second set concentrated on mitigated scenarios.

A widely used lumped parameter model, known as RADMOD [22], was applied to simulate the behaviour of atmospheric and pressurized tanks under fire exposure. Several studies are available in the literature

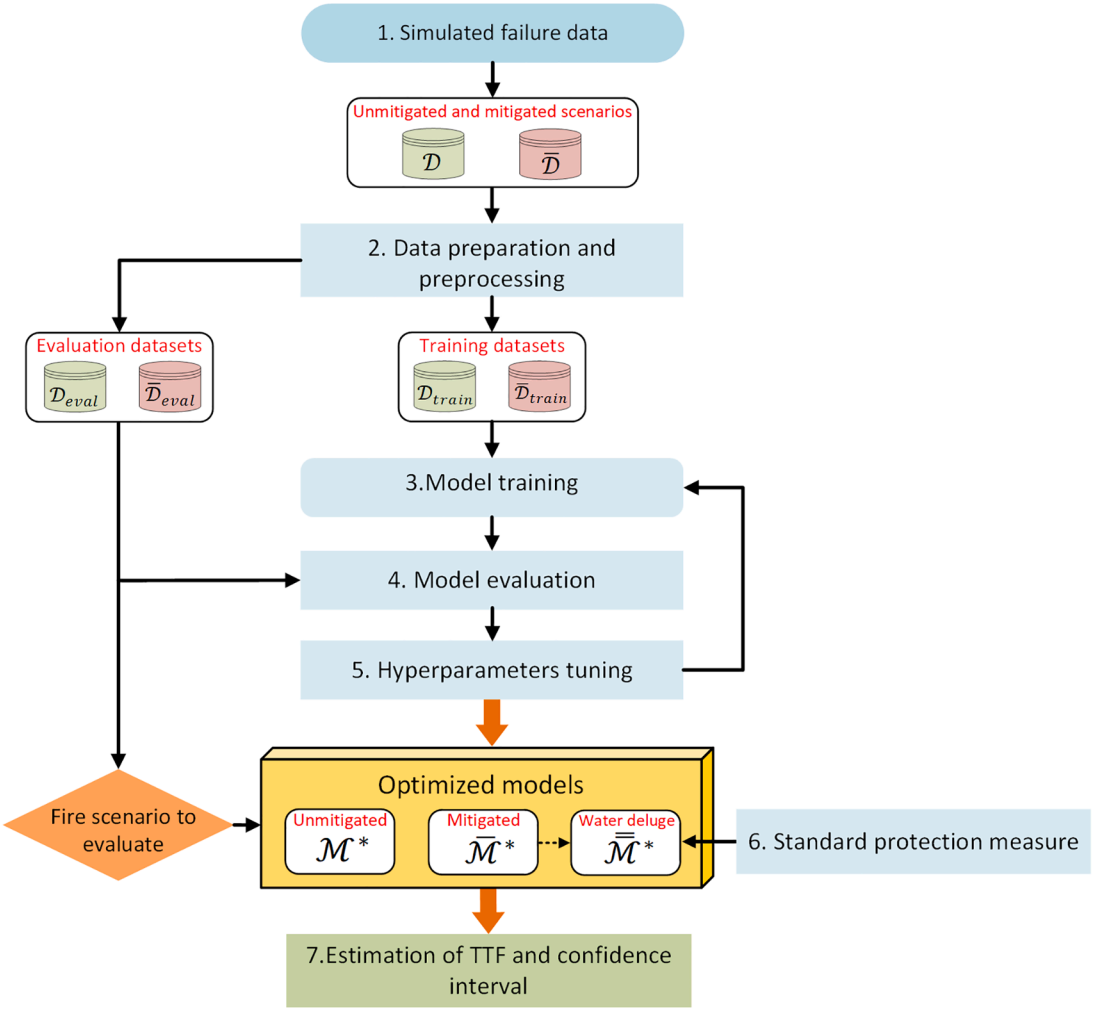

Figure 1. Flowchart of the proposed methodology. $\mathscr{D}_{train}$ and $\overline{\mathscr{D}}_{train}$ indicate the training datasets that contain respectively unmitigated and mitigated fire scenarios. Similarly, $\mathscr{D}_{eval}$ and $\overline{\mathscr{D}}_{eval}$ represent unmitigated and mitigated scenarios used to evaluate the models. $\mathscr{M}^*$ and $\overline{\mathscr{M}^*}$ indicate the models for the prediction of unmitigated and mitigated TTFs. $\overline{\overline{\mathscr{M}^*}}$ represents the simplified model that considers a single standard protection measure (water deluge), introduced as a case study.

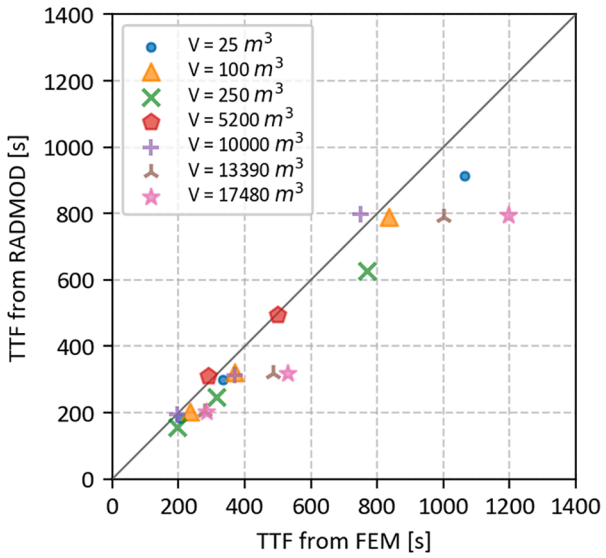

Figure 2. Comparison between the TTF obtained from RADMOD and the TTF obtained from FEM analysis for atmospheric tanks of various volumes [26].

in which this lumped model is applied in the assessment of the TTF for atmospheric tanks exposed to fire (e.g., [21,31,34,56–58]). RADMOD partitions the computational domain into two fluid nodes (the liquid and vapor) and two solid nodes (the liquid-wetted wall and the vapor-wetted wall). It requires specific design (shell diameter, height, and thickness), operational (filling level), and external (heat flux) parameters as inputs. The outputs of the simulations are node temperatures, tank pressure (accounting for the liquid head), axial stress, yield stress, and the equivalent von Mises stress in the steel structure. A detailed description of the RADMOD is reported in [22,26]. The RADMOD model thus retains a limited computational complexity, providing results having an accuracy comparable to that of more complex models. Even if RADMOD shares all the limitations of lumped models, and in particular the impossibility to consider liquid stratification and local temperature gradients on the steel shell, its application to the simulation of the TTF of large atmospheric tanks containing high boiling point liquids exposed to external fires provides sufficiently accurate results, as shown in Fig. 2, showing the results of the model validation against TTF results obtained using finite element analysis (FEM).

The simulation of fire scenarios requires the definition of a set of parameters to describe (i) the tank design and operating parameters, (ii) the characteristics of the external fire, and (iii) the mitigation measures. Table 1 presents a summary of these parameters, along with the corresponding values utilized in the simulations.

The first three parameters in Table 1 define the geometry of the tank. Their values are taken from Table A-2a of API 650: "Welded Steel Tanks for Oil Storage" [59], which defines the shell-plate thickness of typical-sized tanks for oil storage. The table includes a comprehensive list of 136 tank sizes, each characterized by specific values of shell diameter, height, and thickness.

The fourth parameter, filling level, in Table 1 defines the tank filling level, for which three different values were considered: 20%, 50%, or 80%. Therefore, a total of 408 reference tanks were considered for the simulation, each defined by a set of geometric and filling parameters. The internal pressure and temperature were initialized to 1 bar and 20°C, respectively. The substance inside the tank was modelled as benzene, a liquid at 20°C with a density of 878 kg/m^3 and a vapor pressure of 9913 Pa [60].

The fifth parameter, total heat flux, in Table 1 describes the fire conditions defined by the heat flux to the tank wall. Twelve distinct heat flux values were considered, ranging from 10 kW/m^2 to 125 kW/m^2. The lower bound, 10 kW/m^2, corresponds to the radiation threshold at which the TTF of atmospheric equipment exceeds 30 minutes, providing adequate time for effective mitigation without incurring in critical damage [57]. Conversely, the upper bound, 125 kW/m^2, represents a credible heat flux value to a target in severe tank fire scenarios, able to cause target damage in a limited time span, so that effective mitigation is not credible. Thus, the region between the lower and upper bound radiation values identified is that where the accuracy of TTF estimation is more critical in order to assess the time available for effective mitigation and the actual risk of escalation leading to domino effect.

The combination between reference tanks and the fire characteristics led to the definition of 4896 simulated fire scenarios using the RADMOD model. The results were collected in dataset $\mathscr{D}$, which comprises 4896 rows (i.e., number of fire scenarios) and 6 columns; the first 5 columns represent the features of the fire scenario (i.e., diameter, thickness, height, filling level, and total heat flux), while the last column indicates the TTF calculated by the RADMOD model.

An additional set of simulations was performed to incorporate the effects of mitigation measures on the same fire scenarios as defined above. Specifically, the last two parameters in Table 1 define the effect of the safety barriers adopted to mitigate the impact of the fire. The "activation time" represents the time required to activate the barrier, and the "damping factor" indicates the reduction in the total heat load caused by the activation of the safety barrier. Therefore, the net incident radiation at time t can be calculated as

$$\overline{q}(t) = \begin{cases} q & \text{if } t < t_a \\ q(1-\alpha) & \text{if } t \geq t_a \end{cases}, \tag{1}$$

Where $\overline{q}(t)$ indicates the net incident radiation on the tank wall at time t, q represents the total heat flux defined in Table 1, t_a indicates the barrier activation time, and $\alpha \in [0,\ 1]$ is the damping factor. Therefore, the effect of the mitigation measures is to reduce by a factor α the net incident radiation after t_a seconds. Activation time and dumping values were chosen based on reference values for automatic devices, such as fixed water sprays. Specifically, activation times are randomly sampled between 30s and 90s, while dumping factors are sampled between 0.2 and 0.8. Each of the 4896 fire scenarios described earlier was associated with a specific barrier configuration (i.e., t_a and α), and RADMOD was used to simulate the mitigated scenarios. Results were collected in dataset $\overline{\mathscr{D}}$, which contains the TTF values of mitigated scenarios corresponding to the fire scenarios in dataset $\mathscr{D}$. Therefore, the $\overline{\mathscr{D}}$ dataset contains the same number of rows as $\mathscr{D}$, but it has two more columns,

Table 1
The set of variables that defines a fire scenario and their values used in the simulations. * indicates that the values are taken from Table A-2a of API 650 (American Petroleum Institute, 2021)

	Parameter	Values
Tank (geometric)	External diameter* [m]	20 values between 3 and 66
	Wall thickness* [m]	38 values between 0.005 and 0.012
	Height* [m]	10 values between 1.8 and 18
Tank (loading)	Filling level [%]	{20, 50, 80}
Fire	Total heat flux [kW/m^2]	{10, 20, 30, 40, 50, 60, 70, 80, 90, 100, 110, 125}
Mitigation measures	Activation time [s]	Randomly sampled between 30 and 90
	Damping factor	Randomly sampled between 0.2 and 0.8

respectively reporting the activation time and the damping factor of the mitigation measures.

2.2. Data preparation and preprocessing

The two datasets described in the previous section served as the basis for the application of the methodology. However, before developing the machine learning (ML) models, the datasets needed to be preprocessed to arrange the data in a suitable format and facilitate the upcoming analysis. The datasets were split into two parts. The first part was used to train the ML models, while the second was used to evaluate their performance. The dataset $\mathscr{D}$ was split into $\mathscr{D}_{train}$ and $\mathscr{D}_{eval}$, where the former comprises 80% of the scenarios included in $\mathscr{D}$, and the latter contains the remaining observations. Similarly, $\overline{\mathscr{D}}$ was split into $\overline{\mathscr{D}}_{train}$ and $\overline{\mathscr{D}}_{eval}$, respectively comprising 80% and 20% of the events in $\overline{\mathscr{D}}$.

Finally, data were normalized to have zero mean and unit standard deviation. Specifically, a value x in the j-th column of the dataset is normalized as

$$\tilde{x} = \frac{x - \mu_j}{\sigma_j} \tag{2}$$

Where $\tilde{x}$ indicates the normalized value, μ_j represents the mean of column j and σ_j is the standard deviation of column j. This procedure, called Z-score normalization, is a widely used data preprocessing technique that has been demonstrated to improve the generalization and convergence of neural networks [61]. It is worth mentioning that only the features of fire scenarios were normalized (i.e., the TTF was not normalized). In addition, the normalization of the evaluation datasets was performed using the mean and standard deviation of the training datasets to avoid any information leakage between training data and evaluation data.

2.3. Model training

The datasets $\mathscr{D}_{train}$ and $\overline{\mathscr{D}}_{train}$ were used to develop two distinct neural network models. The first model, trained on $\mathscr{D}_{train}$, aims at predicting the TTF of unmitigated fire scenarios. The second model, trained on $\overline{\mathscr{D}}_{train}$, aims at predicting the TTF of mitigated scenarios. The models were developed using Keras version 2.11.0 in Python version 3.10.11.

In this study, Fully-Connected Feed-Forward Neural Networks (FC-FFNNs) were used to model the relationship between scenario features and the TTF. FC-FFNNs were preferred over other conventional regression models (e.g., Linear regression, Support Vector Regression) due to their excellent abstraction and generalization capabilities [61,62]. In addition, FC-FFNNs offer a good balance between simplicity and effectiveness, making them an ideal choice over more advanced and complex algorithms. In fact, FC-FFNNs are less computationally demanding, making them suitable when computational resources are limited or for tasks that do not require complex models. FC-FFNNs also tend to generalize well and are less prone to overfitting, especially with limited data. Their training is more straightforward, involving fewer hyperparameters, which saves time and effort in model development. A schematic representation of an FC-FFNN is presented in Fig. 3.

FC-FFNNs are directed acyclic graphs that comprise an input layer (orange in Fig. 3), one or more hidden layers (blue in Fig. 3), and one output layer (green in Fig. 3). Each layer comprises one or more units (circles in Fig. 3), which are real-valued entities. The units of the input layer are the features of an observation (e.g., the parameters in Table 1). In contrast, the units of the hidden layers, also called hidden units or hidden neurons, are calculated through a nonlinear transformation of the linearly combined units in the previous layers [62]. Specifically, a generic layer $Z_i \in \mathbb{R}^{M\times 1}$ with M neurons is computed as follows:

$$Z_i = \sigma(W_i \cdot Z_{i-1} + b_i), \tag{3}$$

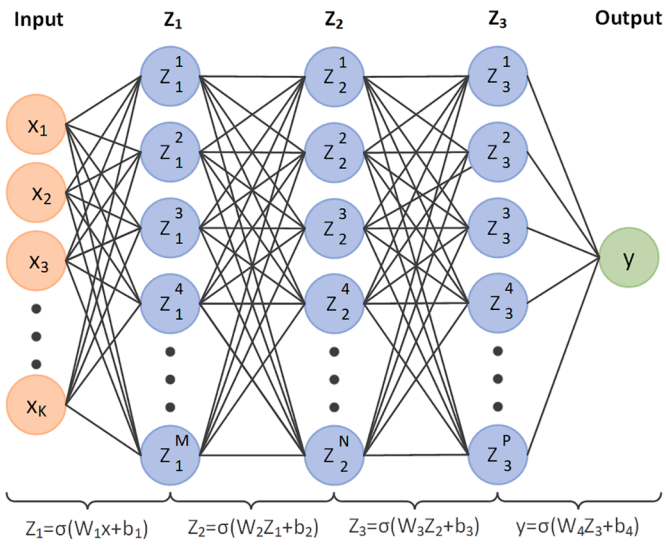

Figure 3. A schematization of an FC-FFNN with three hidden layers. The input of the model (i.e., the features) is depicted in orange. Hidden layers (Z_i) and units (Z_i^j) are represented in blue. The model output (i.e., the response) is depicted in green.

Where σ is the rectified linear unit (ReLu) function [63], $W_i \in \mathbb{R}^{N\times M}$ is the matrix of the weights, $Z_{i-1} \in \mathbb{R}^{N\times 1}$ is the layer preceding Z_i, and $b_i \in \mathbb{R}^{M\times 1}$ is the vector of the biases. Weights and biases are learnable parameters that are tuned during training. The network's last layer is the output layer (green in Fig. 3), representing the response variable (i.e., the TTF). Therefore, the NN aims at identifying the function f that approximates the relationship between features and response:

$$y \approx f(x) \tag{4}$$

The function f comprises a set θ of learnable parameters, namely the weights and the biases introduced in Eq. (3). Such parameters are randomly initialized and eventually tuned during the training procedure to minimize the error between the model's predictions and the actual value of the TTF. The training dataset (i.e., $\mathscr{D}_{train}$ or $\overline{\mathscr{D}}_{train}$) are used to train the models. Specifically, examples of both features and related TTFs are fed to the model. The model uses the features to calculate the predicted TTF, which is compared to the actual TTF, and the resulting error is back-propagated to update the learnable parameters θ. The procedure is iterative and aims to find the best set of hyperparameters, θ^*, that minimizes the error between predicted TTFs ($\tilde{y}$) and true TTFs (y),

$$\theta^* = \underset{\theta}{argmin}[\ell(y,\ \tilde{y}(\theta))], \tag{5}$$

Where ℓ indicates the "loss", a function that measures the error between predictions and true responses. In this study, the mean squared error (MSE), defined as $MSE = 1/N\sum_{i=1}^{N}(y_i - \tilde{y}_i)^2$, is used as a loss function, where $N \in \mathbb{N}$ is the number of scenarios included in the training datasets. The MSE is a differentiable loss function, which helps with network convergence. However, it is highly susceptible to the presence of outliers, as they have the potential to heavily distort the squared differences between predicted and actual values, resulting in inflated error measurements. In the datasets utilized for this study, outliers are not present, thereby making the MSE an appropriate choice as a loss metric.

As mentioned earlier, $\mathscr{D}_{train}$ or $\overline{\mathscr{D}}_{train}$ are utilized to construct two independent models, namely $\mathscr{M}$ and $\overline{\mathscr{M}}$, where their parameters are optimized to predict the TTF of unmitigated and mitigated fire scenarios, respectively. Assuming a successful training procedure, the

models should be capable of predicting the TTF of fire scenarios contained in $\mathscr{D}_{train}$ or $\overline{\mathscr{D}}_{train}$ with minimal error. However, there is no guarantee that the models will maintain the same level of accuracy when considering new fire scenarios. Hence, evaluating the models using independent scenarios is crucial to ensure their ability to generalize the knowledge acquired during training to previously unseen events. The evaluation procedure will be described in the following section.

2.4. Model evaluation

The trained models are evaluated on their ability to predict the TTF of scenarios included in $\mathscr{D}_{eval}$ and $\overline{\mathscr{D}}_{eval}$. The features of the fire scenarios included in $\mathscr{D}_{eval}$ are fed to the model $\mathscr{M}$, which predicts the TTFs based on the knowledge extracted from $\mathscr{D}_{train}$. Similarly, the model $\overline{\mathscr{M}}$ is evaluated on $\overline{\mathscr{D}}_{eval}$. It is worth noting that only the features of fire scenarios are fed to the model during the evaluation phase, as opposed to the training phase, where both features and TTFs were used.

The evaluation of the models involves the calculation of performance metrics to quantify the quality of predictions. In this study, we utilize the following metrics:

- Coefficient of determination (R^2)

$$R^2 = 1 - \frac{\sum_{i=1}^{M}(y_i - \tilde{y}_i)^2}{\sum_{i=1}^{M}(y_i - \mu)^2} \tag{6}$$

  Where, $M \in \mathbb{N}$ is the number of fire scenarios included in the evaluation dataset, y_i and $\tilde{y}_i$ are respectively the true and predicted TTF values, and μ is the mean of the true TTFs.
- Root mean squared error (RMSE)

$$RMSE = \sqrt{\frac{1}{M}\sum_{i=1}^{M}(y_i - \tilde{y}_i)^2} \tag{7}$$

Typically, the coefficient of determination assumes values between 0 and 1, although negative values are possible when the model performs worse than a constant function that simply predicts the mean of the data. Values of R^2 close to 1 are often interpreted as a good quality of the fit, which is generally true. However, it is important to remark that there may be specific circumstances in which large R^2 values do not necessarily guarantee the usefulness of the regression model [64].

For this reason, the RMSE is also considered to overcome the limitations of R^2. The *RMSE* may be interpreted as the square root of the variance of the residual. Therefore, it indicates how spread out these residuals are. This metric is bounded below by 0 but has no upper bound. Values of *RMSE* close to 0 indicate good prediction performances. However, it must be noted that *RMSE* shares the same units as the response variable (e.g., "seconds" for TTF). Therefore, when evaluating model performance, it is essential to consider the magnitude of the response variable in comparison to the *RMSE*. Often, to remove the effect of scale and enable a fair comparison between models trained on different tasks, the *RMSE* is normalized using the mean of the response variable. This normalized version is usually defined as the normalized RMSE (NRMSE):

$$NRMSE = \frac{RMSE}{\mu} \tag{8}$$

If the objective is to compare the performance of two or more models on the same task, the RMSE can be used directly. In such cases, the model with the lowest RMSE is considered to outperform the other models.

2.5. Hyperparameters tuning

The procedures described in Sections 2.3 and 2.4 illustrate how to train and evaluate the models $\mathscr{M}$ and $\overline{\mathscr{M}}$ for predicting the TTF of unmitigated and mitigated scenarios. However, no details about the network hyperparameters have been provided. The hyperparameters of a NN may be defined as non-trainable parameters that define its structure and behaviour during training [65]. For example, the number of hidden layers and neurons per layer are hyperparameters that can significantly influence the model's performance. Unfortunately, selecting the right set of hyperparameters is mainly guided by background knowledge and experimentation [66], and there is no "golden rule" to define an optimal set of hyperparameters in hindsight.

In this study, a "grid-search" procedure [67] was used to tune the network hyperparameters. This procedure involves (i) defining a search space for each parameter, (ii) training and evaluating one model for each unique combination of hyperparameters, and (iii) comparing the performance of the models and selecting the best set of hyperparameters.

The search space is defined by specifying the range or discrete values for each hyperparameter under consideration. In this study, we focus on three hyperparameters: the number of layers, the number of neurons per layer, and the learning rate (LR). The number of layers and neurons defines the network structures, as discussed in Section 2.3. The Learning Rate is a key parameter determining the step size at which the model updates its parameters during training. A large learning rate increases the convergence speed but raises the risk of the model diverging and failing to converge to an optimal solution. The search space used in this study is defined in Table 2.

The combination of the hyperparameters leads to the definition of 5600 model configurations, each characterized by several layers, one or more neurons per layer, and one learning rate. The grid search algorithm systematically evaluates the model performance for every possible combination within the defined search space. Specifically, each model configuration is used to train and assess the models $\mathscr{M}$ and $\overline{\mathscr{M}}$ as described in Sections 2.3 and 2.4. The training procedure was conducted with 300 epochs, which indicates the number of iterations made by the model over the training dataset. The selected number of epochs represents a good balance between computational complexity and model accuracy. A larger number of epochs would significantly increase the computation time, while fewer epochs may penalize the complex models with low learning rates because they typically require more training samples to perform adequately.

As a result, every model configuration is associated with an *RMSE* value that reflects its performance in predicting the TTF for unmitigated events, as well as another *RMSE* value for predicting mitigated TTFs. The model that obtains the lowest *RMSE* on $\mathscr{D}_{eval}$ identifies the best configuration for the prediction of unmitigated TTFs, while the model that obtains the lowest *RMSE* on $\overline{\mathscr{D}}_{eval}$ identifies the best configuration for the prediction of mitigated TTFs. The two tasks (i.e., prediction of the TTF for unmitigated and mitigated scenarios) are treated independently because there is no guarantee that the best model for the prediction of unmitigated TTFs will also show superior performance on the prediction of mitigated TTFs [68].

The grid search procedure creates two models optimized for predicting the TTF of unmitigated and mitigated scenarios. The first model, namely $\mathscr{M}^*$, takes as an input the first five parameters in Table 1, while the second model, namely $\overline{\mathscr{M}}^*$, requires the complete set of parameters.

Table 2
The search space used in the grid-search procedure.

Hyperparameter	Values
Number of layers	{1, 2, 3, 4}
Number of neurons per layer	{2, 52, 102, 152, 202, 252, 302}
Learning Rate	{0.01, 0.001}

It is worth mentioning that the selection of the search space in Table 2 has been mainly guided by background knowledge, and it is not meant to identify the best model in absolute terms. In fact, there are additional hyperparameters that may require training, such as the choice of the activation function (σ in Eq. (3)), and other parameters not covered in this study, including batch size, regularization layers, and optimizers [65]. Nonetheless, the search space in Table 2 encompasses the parameters that the authors consider as the most crucial for addressing the specific task at hand, striking a balance between model performance and computational efficiency as the inclusion of additional hyperparameters in the search space can lead to a significant increase in computational requirements.

2.6. Definition of a standard protection measure

The model $\overline{\mathscr{M}^*}$ for evaluating mitigated scenarios, requires defining the activation time and damping factor of the protection measure, as discussed in Section 2.1. These characteristics are site-specific and depend on the particular fire detection and protection systems implemented. Therefore, there might be instances where they cannot be easily obtained. For these reasons, a third model was developed to predict the TTF of mitigated scenarios, namely $\overline{\overline{\mathscr{M}^*}}$, which considers a reference protection measure with standard activation time and damping factor. The model is intended to provide a rough estimate of the potential effect of mitigation systems based on the performance of a reference active barrier widely used in the current industrial practice. The model was obtained from $\overline{\mathscr{M}^*}$ selecting the activation time and the damping factor of a water deluge system. The activation time was set to 1 minute, which included 30 seconds to detect the fire and 30 seconds to activate water delivery to the nozzles [69]. The damping factor is set to 0.2, which corresponds to a single row of nozzles, as reported by Lowesmith et al. [70] and in accordance with the simulations carried out by Wu et al. [71].

The third model offers a generic reference estimation of the TTF for mitigated tanks, based on the standard performance of water deluges. The model only intends to provide preliminary results when activation times and damping factors of the actual mitigation barriers are unavailable, e.g., when considering installing protection measures in a preliminary design phase. If the actual activation times and damping factors are known, model $\overline{\mathscr{M}}$ must be used since it provides far more accurate data.

2.7. Predictions and confidence intervals

The optimized models $\mathscr{M}^*$ and $\overline{\mathscr{M}^*}$, can predict the TTF of unmitigated and mitigated scenarios. Furthermore, the specialized model $\overline{\overline{\mathscr{M}^*}}$ can be used to simulate the effect of a standard water deluge system. However, in most practical applications, predicting a confidence interval rather than a single precise value for the TTF is often preferable. This is because confidence intervals provide a range of potential values that captures the uncertainty and variability associated with the prediction. In fact, if a fire scenario differs significantly from those used during training, it is reasonable to expect larger uncertainties associated with the prediction of the TTF. In such cases, it becomes crucial to acknowledge the potential uncertainties and incorporate a larger confidence interval in the prediction.

This study used a model-agnostic method called "jacknife+" to estimate predictive confidence intervals [72]. The confidence interval produced by jacknife+ can be summarized as follows. Let X_i and y_i respectively indicate the features and the response variable of the i-th observation in a training dataset that comprises n samples. The confidence interval of a new observation X_{n+1} is defined as:

$$\widehat{C}_{n,\alpha} = \left[\widehat{q}^{-}_{n,\alpha}\left\{\widehat{\mu}_{-i}(X_{n+1}) - R_i^{LOO}\right\},\ \widehat{q}^{+}_{n,\alpha}\left\{\widehat{\mu}_{-i}(X_{n+1}) - R_i^{LOO}\right\}\right], \tag{9}$$

where $\widehat{C}_{n,\alpha}$ indicates the confidence interval in the form [TTF_{min}, TTF_{max}], $\alpha \in [0,1]$ indicates the uncertainty of the confidence interval, $\widehat{q}^{-}_{n,\alpha}[\bullet]$ and $\widehat{q}^{+}_{n,\alpha}[\bullet]$ respectively represents the α and 1- α quantiles, $\widehat{\mu}_{-i}$ is the regression model fitted on all the examples in the training database except the i-th observation, and $R_i^{LOO} = |y_i - \widehat{\mu}_{-i}(X_i)|$ is the residual of the i-th observation. A detailed description of the theoretical foundations and implementation of the method can be found in the original reference [72] and the Python library description [73]. In summary, the jacknife+ method extends the traditional jacknife resampling technique [74] by addressing algorithm instability, offering robust coverage guarantees without requiring any assumptions apart from having independent and identically distributed samples.

Therefore, incorporating the jacknife+ method, the output of the models $\mathscr{M}^*$, $\overline{\mathscr{M}^*}$, and $\overline{\overline{\mathscr{M}^*}}$ includes not only the predicted TTF but also the corresponding minimum and maximum TTF values, indicating that the true TTF is expected to lie between these two values with a confidence level of 95%.

3. Results

The best model configurations identified by the grid-search procedure (see Section 2.5) are shown in Table 3. The table reports the determination coefficient, R^2, and the root mean squared error, *RMSE*, that may be considered as the main performance metrics of the model. The results reported in Table 3 indicate that the model for predicting unmitigated scenarios ($\mathscr{M}^*$) achieves lower *RMSE* and larger R^2 than the model that predicts mitigated scenarios ($\overline{\mathscr{M}^*}$ and $\overline{\overline{\mathscr{M}^*}}$). However, the TTFs of mitigated scenarios are expected to be higher than those of unmitigated scenarios. Therefore, the *RMSE* was normalized to remove the effect of scale and to allow a fair comparison between the models.

Figs. 4 and 5 provide illustrative examples of the model output, intended to exemplify the potential use of the unmitigated ($\mathscr{M}^*$) and mitigated ($\overline{\mathscr{M}^*}$, $\overline{\overline{\mathscr{M}^*}}$) models, and to demonstrate their accuracy and robustness under different working conditions. A reference tank containing benzene at 20°C and 1 atm, with diameter = 6 m, height = 14.4 m, shell thickness = 0.005 m, filling level = 20 %, and a total heat flux = 50 kW/m^2 is used for the analysis. It is important to remark that both the tank geometry and the fire radiation considered were not included in the training sets.

Each plot in Figs. 4 and 5 shows the effect of a single feature of the scenario (see Table 1) while holding the others constant. In particular, in Fig. 4, the TTF values obtained using model $\mathscr{M}^*$ for unprotected tanks are reported with respect to thermal radiation (a), shell diameter (b), shell thickness (c), tank height (d), and filling degree (e). The shell thickness of the reference tank was increased to 0.01 m in Fig 4b in order to ensure physical integrity across the whole range of shell diameters. As shown in the figure, the model predicted values (predicted TTF) show a good agreement with the results of the RADMOD model (true TTF) across the entire feature space. The relatively small confidence intervals indicate low uncertainty in the predictions. The computation time required to perform one prediction is approximately 23.7 milliseconds for both models.

Table 3
Best model configurations for the prediction of mitigated and unmitigated TTFs. R^2 and RMSE are calculated according to Eq. (6) and (7), NRMSE is calculated according to Eq. (8).

Model	Layers	Neurons	R^2	*RMSE* [s]	*NRMSE*
$\mathscr{M}^*$ (unmitigated)	2	{152, 52}	0.9999	1.66	0.006
$\overline{\mathscr{M}^*}$ and $\overline{\overline{\mathscr{M}^*}}$ (mitigated)	3	{102, 152, 2}	0.9925	71	0.124

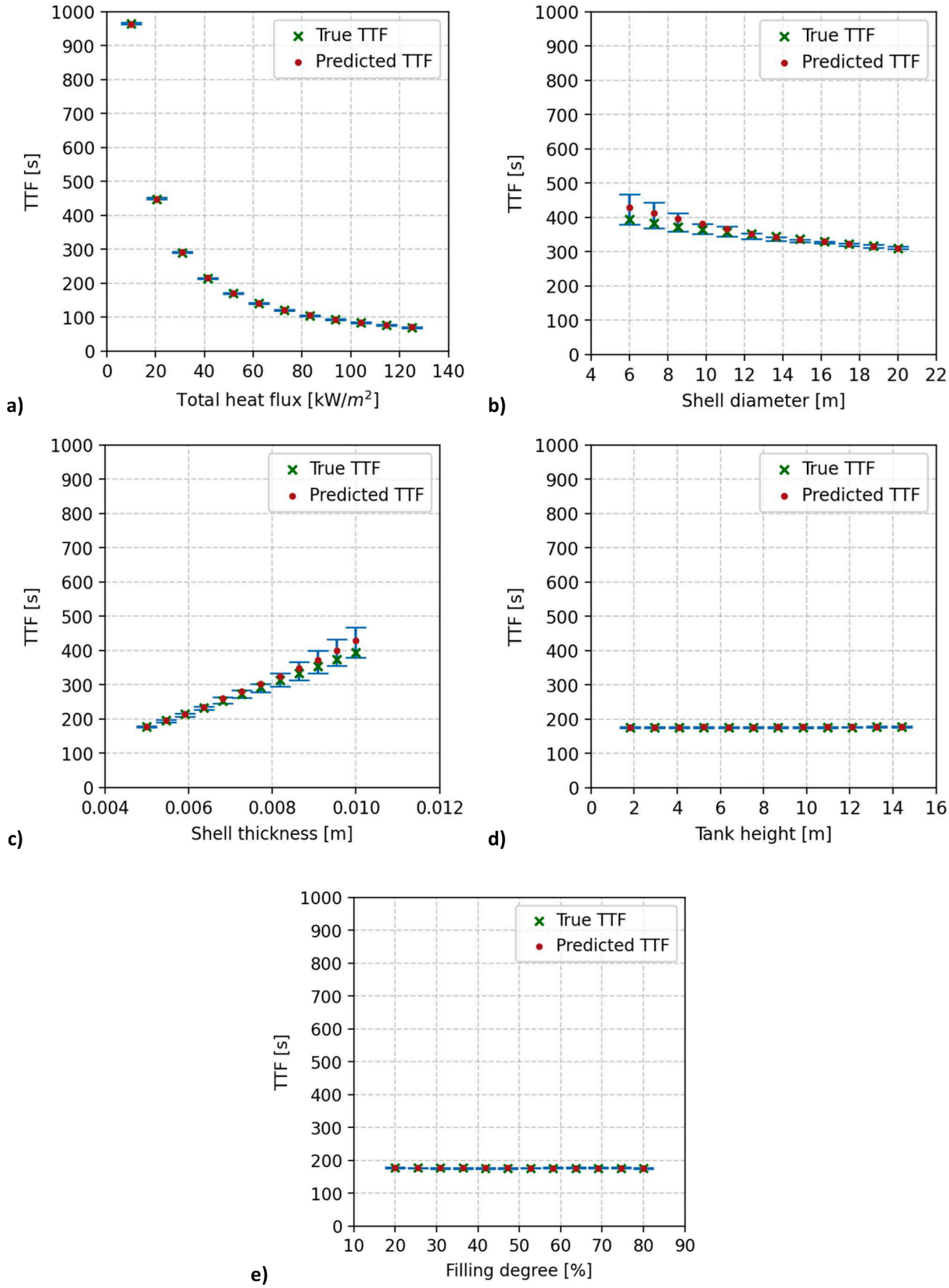

Figure 4. TTF values calculated by model $\mathscr{M}^*$ for an unmitigated tank with diameter = 6 m, height = 14.4 m, shell thickness = 0.005 m, filling level = 20 %, containing benzene initially at 20°C and 1 bar, exposed to a total heat flux = 50 kW/m^2. Each plot examines the effect of a specific tank feature while holding the others constant: (a) total heat flux, (b) diameter, (c) thickness, (d) height, and (e) filling degree.

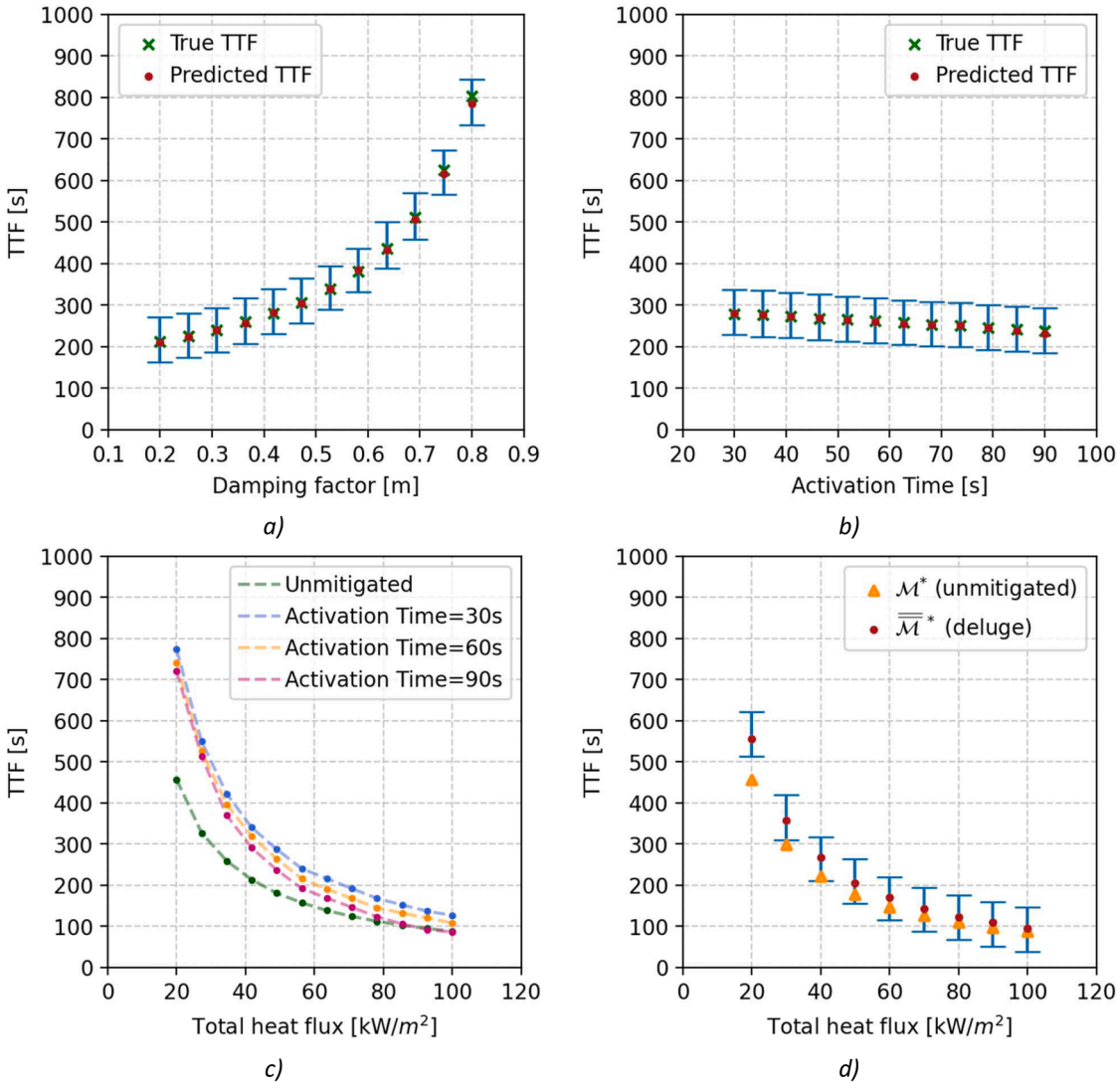

Figure 5. TTF values calculated by model $\overline{\mathcal{M}}^*$ (a, b,c) and model $\overline{\overline{\mathcal{M}}}^*$ (d) for a mitigated tank with diameter = 6 m, height = 14.4 m, shell thickness = 0.005 m, filling level = 20 %, total heat flux = 50 kW/m^2, activation time = 40 s, damping factor = 0.4, and containing benzene initially at 20°C and 1 bar. Panels a and b examine the effect of the damping factor (a) and activation time (b) while holding the other tank characteristics constant. Panel c illustrates the combined effect of varying the activation time and the total heat flux. Panel d shows the comparison of the TTF for an unmitigated fire and a fire mitigated by water deluges.

The analysis of mitigated model results is shown in Fig. 5. Specifically, Fig. 5.a illustrates the TTF values versus the damping factor calculated considering an activation time of 40 seconds. Fig. 5b shows the effect of activation time considering a safety barrier with damping factor equal to 0.4. Also in this case a good agreement with simulated data is present, even if confidence intervals are larger, indicating that the model $\overline{\mathcal{M}}^*$ is associated with higher uncertainties. Fig. 5c compares the TTF values calculated by the model $\mathcal{M}^*$ for an unmitigated tank, and model $\overline{\overline{\mathcal{M}}}^*$ that considers the reference water deluge system introduced in section 2.6. As shown in the figure, the presence and activation of the water deluge results in a relevant increase of TTF values (up to 27 %) with respect to the values calculated for unmitigated tanks. The difference is larger for lower values of heat radiation and rapidly decreases as the heat load increases. The trend can be attributed to the intensified influence of higher heat loads before barrier activation (i.e., during the initial 60 seconds), rapidly pushing the tank closer to its mechanical limits and thus diminishing the benefits of the water deluge system.

Figs. 4 and 5 evidence the strong non-linear correlation among the TTF and thermal radiation, corroborating the findings from Landucci et al. [26]. Thus, the effect on the TTF of the dynamic behaviour of thermal radiation induced by the presence of mitigation systems and by environmental facts is complex. Models based on the thermal dose concept, as that of Zhou et al. [75], were proposed to capture such effects, but the discussion of such approaches falls out of the scope of the present paper.

The analysis of mitigated model results is shown in Fig. 5. Specifically, Fig. 5a illustrates the TTF values versus the damping factor calculated considering an activation time of 40 seconds. Fig. 5b shows the effect of activation time considering a safety barrier with damping factor equal to 0.4. Also in this case a good agreement with simulated data is present, even if confidence intervals are larger, indicating that the model $\overline{\mathcal{M}}^*$ is associated with higher uncertainties. Fig. 5c compares the TTF values calculated by the model $\mathcal{M}^*$ for an unmitigated tank, and model $\overline{\overline{\mathcal{M}}}^*$ that considers the reference water deluge system introduced in section 2.6. As shown in the figure, the presence and activation of the water deluge results in a relevant increase of TTF values (up to 27 %) with respect to the values calculated for unmitigated tanks. The difference is larger for lower values of heat radiation and rapidly decreases as the heat load increases. The trend can be attributed to the intensified influence of higher heat loads before barrier activation (i.e., during the

initial 60 seconds), rapidly pushing the tank closer to its mechanical limits and thus diminishing the benefits of the water deluge system.

Fig. 5c shows the combined effect of the heat radiation intensity and of the barrier activation time on the TTF. As expected, the results confirm that the TTF increases as the activation time of the barrier decreases. The effect is more relevant at high values of the heat radiation, where the TTF is lower and the activation time approaches the TTF of the unmitigated scenario. Nevertheless, when the activation time equals the TTF of the unmitigated fire scenarios, the mitigated and unmitigated TTF values coincide (since actually the mitigation starts after tank failure). This observation also underscores a good agreement between the mitigated and unmitigated models, as they produce comparable TTF values when the barrier activation time coincides with the unmitigated TTF.

To gain further insights into the performance of the models, the distribution of residuals was calculated for both models $\mathscr{M}^*$ and $\overline{\mathscr{M}^*}$. The results are illustrated in Fig. 6a and Fig. 6b, respectively.

Residuals represent the difference between actual and predicted TTFs of the fire scenarios in the evaluation dataset. Fig. 6a shows that most residuals of the model $\mathscr{M}^*$ are smaller than 10 seconds in absolute terms. Only one prediction returned a residual of -15 seconds. Also, the distribution appears centered around 0, with most residuals between -5 and +5 seconds. Similarly, Fig. 6b shows that most residuals of the model $\overline{\mathscr{M}^*}$ are close to 0, but the distribution appears more skewed toward negative values, with three outliers around -973, -673, and -378 seconds.

A comprehensive analysis was conducted to compare the model performance $\mathscr{M}^*$, with the simplified correlations proposed by Landucci et al. [26] and Yang et al. [27]. The models were tested based on the ability to predict the TTFs of the unmitigated fire scenarios included in $\mathscr{D}_{eval}$ dataset (see section 2.2). A comparison between the RMSE values obtained by the model $\mathscr{M}^*$ and the correlations by Landucci et al. [26] and Yang et al. [27] is shown in Table 4. The results show that while the model of Yang et al. [27] has a slightly better performance than that of Landucci et al. [26], the new model developed outperforms the previous approaches. Specifically, it reduces the Root Mean Square Error (RMSE) by an order of magnitude compared to the correlations by Landucci et al. [26] and Yang et al. [27].

A comparison between the three models is offered in Fig. 7, showcasing 'predicted versus actual' plots the new model developed in the present study to that of Landucci et al. [26] (Fig. 7a) and of Yang et al. [27] (Fig. 7b).

Table 4
Comparison between RMSE values obtained by the model presented in this study and state-of-the-art correlations. Only the events include $\mathscr{D}_{eval}$ were considered in the analysis.

Approach	RMSE [s]
The present study	1.66
Landucci et al. [26]	162.9
Yang et al. [27]	106.4

The results confirm that the model proposed in this study aligns remarkably well with the RADMOD data, exhibiting a high accuracy in reproducing RADMOD results. On the contrary, the correlations proposed by Landucci et al. [26] and Yang et al. [27] result in larger errors, in particular when high values of TTFs are considered.

4. Discussion

The results presented above indicate that the models developed in the present study effectively predict the time-to-failure (TTF) of atmospheric tanks exposed to external fire, using a minimal set of input data and requiring a reduced computational effort. This approach provides safety practitioners and researchers with models that are not only user-friendly and accurate but also highly interpretable. Additionally, the seamless integration of safety barriers within this framework represents a notable advancement in the risk assessment of fire-induced domino scenarios.

The results indicate that the models show a relatively good performance. However, model $\mathscr{M}^*$ (that considers unprotected tanks) exhibits a higher robustness and accuracy with respect to models $\overline{\mathscr{M}^*}$ and $\overline{\overline{\mathscr{M}^*}}$ (that consider the effect of safety barriers), as confirmed by the smaller confidence intervals in Fig. 4 and by the distributions of the residuals shown in Fig. 6. The better performance of the model predicting the TTF values for unmitigated fire scenarios can be attributed to the challenge of predicting the effects of safety barriers with variable activation times and damping factors. This complexity demands a more sophisticated approach to accurately capture the impact of safety measures, as evidenced by the need for additional layers and neurons per layer, as shown in Table 3.

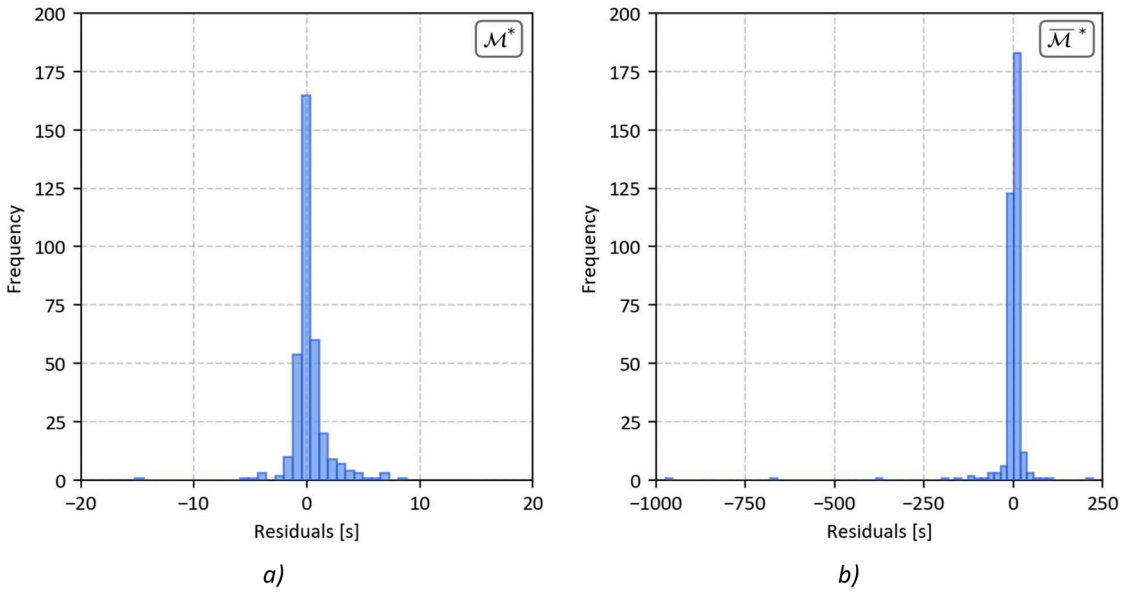

Figure 6. Residuals of the model $\mathscr{M}^*$(a) and $\overline{\mathscr{M}^*}$(b). Residuals are calculated as the difference between the true TTF and the predicted TTF of fire scenarios included in the evaluation datasets.

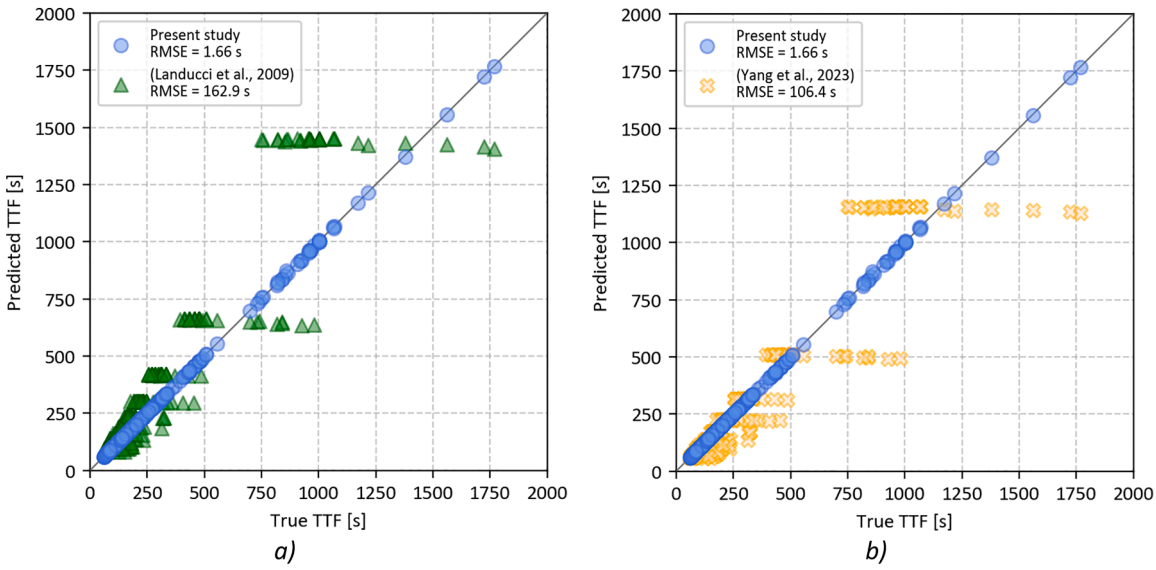

Figure 7. Comparison between the performance of the model $\mathscr{M}^*$ (blue), the simplified correlations proposed by Landucci et al. [26] (a) and the correlation proposed by Yang et al. [27] (b). Displayed TTFs refer to unmitigated scenarios included in the $\mathscr{D}_{eval}$ dataset (see Section 2)

The results presented in Figs. 4 and 5 provide some key insights into the factors influencing the TTF in the given scenarios. The analysis shows that the total heat flux, along with the shell diameter and thickness, have a great influence on the TTF. Conversely, the height of the tank and its filling degree have a less significant, almost negligible, impact. Considering the effect of safety barriers, Fig. 5 suggests that the damping factor exerts a more substantial influence than the activation time. It is imperative to stress that a careful and accurate assessment of the activation time, particularly in comparison to the TTF in unmitigated fire scenarios, is a key determinant of the barrier effectiveness.

The NN model addressing the simulation of unmitigated scenarios ($\mathscr{M}^*$) outperforms the simplified correlations reported in the literature [21,26], which are not conceived to capture the dynamics of the fire scenarios. Also, the simplified correlations do not consider the effect of the tank filling degree. In contrast, the proposed models may be easily tailored to the specific case of interest, is accurate, and provides results rapidly, requiring limited computational resources. Thus, the NN models are excellent candidates for dynamic frameworks to assess safety barriers and the risk generated by potential escalations resulting in domino scenarios.

Despite these promising results, it is important to acknowledge some limitations of the NN models developed and some potential areas for future improvements. Firstly, the models were trained using data from a simplified lumped model (i.e., RADMOD), which may, in turn, introduce errors in estimating the TTF values. Incorporating more rigorous TTF data, such as those obtained from large-scale experimental set-ups and/or validated CFD and FEM models, could enhance the performance of the NN models. In this context, the approach shown in the present study demonstrates the potential of coupling first principles modelling and ML for the construction of metamodels that can offer fast and reliable predictions, thereby decreasing the computational burden of techniques requiring many simulations.

Another limitation that needs to be pinpointed is the larger uncertainty associated with the TTF calculated from the model considering mitigated scenarios with respect to those obtained from the model considering unprotected tanks. Future work should focus on exploring a more extensive set of data and hyperparameters, including regularization layers, on enhancing the performance of $\overline{\mathscr{M}^*}$.

In addition, it is crucial to emphasize that the models developed in this study are intended as surrogate tools to calculate the Time to Failure (TTF) and are not meant to replace comprehensive dynamic risk analysis procedures. Fire spread and evolution are intricate phenomena shaped by a multitude of factors. Actually, both environmental aspects, as atmospheric conditions and the tank position relative to the fire, and human factors, such as individual behaviours and the timeliness and efficacy of emergency response, influence the fire scenario. The factors that influence the fire intensity, such as the type of ignited substance, air transmissivity, and view factor must be considered in models addressing the simulation of the fire scenario. To this end, several literature models provide correlations that can be used to link environmental aspects to the total incident radiation (e.g. see [76]). Furthermore, comprehensive frameworks are available to address the dynamic evolution of fire scenarios also considering emergency response [30,77]. Such models provide the intensity of the thermal radiation and the duration of the fire, that are input parameters to the models developed in the present study, focusing on the improved estimation of TTF also considering mitigation measures. Environmental and human factors shall thus be considered upstream, prior to the application of the models developed, allowing for a more targeted and effective integration into the overall risk assessment process.

Finally, it is worth mentioning that the models proposed in this study are not specifically designed to provide conservative predictions, as indicated by the residuals in Fig. 6. The figure shows that the errors are likely to be both negative or positive, meaning that the predicted TTF is not always guaranteed to be smaller than the true TTF. This behaviour is at least in part mitigated by the confidence intervals, which offer an estimation of the uncertainty affecting the TTF. The confidence interval allows a better understanding of the robustness of the predictions, allowing more informed judgments based on the level of confidence associated with the prediction.

Despite the abovementioned limitations, this study provides accurate and user-friendly tools, enabling a straightforward evaluation of fire scenarios under mitigated and unmitigated conditions. The toolbox of developed models may thus significantly benefit the assessment of domino scenarios triggered by the fire. The model's capabilities in predicting TTFs for atmospheric tanks and considering the effect of mitigation systems provide new opportunities to enhance the risk assessment and safety evaluation of cascading events leading to domino effects. From a practitioners' viewpoint, the availability of a toolbox of user-friendly models, able to incorporate the effect of mitigation measures without the need of a specific expertise, provides a crucial support

to risk-informed decision-making in displaying safety barriers and safety systems aimed to prevent escalation and domino effect.

5. Conclusions

This study is pioneering in proposing using Neural Networks to estimate the TTF of atmospheric tanks exposed to external fires, also considering the effect of mitigative actions. A model toolbox was developed, including NN-based modes allowing the TTF calculation for unprotected tanks and for tanks protected by active and/or passive safety barriers. The models consider the effect of various types of safety measures and safety systems in terms of activation time and effectiveness in reducing the heat load, thus allowing the simulation of a wide range of safety barriers. The models require only a minimal set of input parameters, thus resulting user-friendly and straightforward to configure. The predictions are fast and accurate, making the models suitable for the dynamic analysis of domino scenarios. The newly developed NN-based models outperform the simplified correlations used in the current practice to estimate TTF, allowing a more accurate calculation of TTF values. Overall, the method demonstrates the potential of coupling digital simulations and ML models to decrease the computational burden, enabling faster and more efficient predictions in complex accident scenarios.

CRediT authorship contribution statement

Nicola Tamascelli: Writing – original draft, Software, Methodology, Investigation, Data curation, Conceptualization. **Giordano Emrys Scarponi:** Writing – original draft, Methodology, Investigation, Data curation, Conceptualization. **Md Tanjin Amin:** Validation, Investigation, Conceptualization. **Zaman Sajid:** Writing – review & editing, Validation, Investigation. **Nicola Paltrinieri:** Writing – review & editing, Validation, Methodology. **Faisal Khan:** Writing – review & editing, Supervision, Investigation, Conceptualization. **Valerio Cozzani:** Writing – review & editing, Supervision, Methodology, Conceptualization.

Declaration of competing interest

The authors declare that they have no known competing financial interests or personal relationships that could have appeared to influence the work reported in this paper.

Data availability

Data will be made available on request.

Supplementary materials

Supplementary material associated with this article can be found, in the online version, at doi:10.1016/j.ress.2024.109974.

References

[1] Vipin, Pandey SK, Tauseef SM, Abbasi T, Abbasi SA. Pool fires in chemical process industries: occurrence, mechanism, management. J Failure Anal Prevent 2018;18:1224–61. https://doi.org/10.1007/s11668-018-0517-2.

[2] Lees F. Fire. Lees' loss prevention in the process industries. Elsevier; 2012. p. 1075–366. https://doi.org/10.1016/B978-0-12-397189-0.00016-1.

[3] Abdolhamidzadeh B, Abbasi T, Rashtchian D, Abbasi SA. Domino effect in process-industry accidents – An inventory of past events and identification of some patterns. J Loss Prev Process Ind 2011;24:575–93. https://doi.org/10.1016/j.jlp.2010.06.013.

[4] Huang K, Chen G, Khan F, Yang Y. Dynamic analysis for fire-induced domino effects in chemical process industries. Process Saf Environ Protect 2021;148:686–97. https://doi.org/10.1016/j.psep.2021.01.042.

[5] Naderpour M, Khakzad N. Texas LPG fire: domino effects triggered by natural hazards. Proc Saf Environ Protect 2018;116:354–64. https://doi.org/10.1016/j.psep.2018.03.008.

[6] Fishwick T. The fire and explosion at Indian Oil Corporation, Jaipur — a summary of events and outcomes. Loss Prevent Bull 2011:9–13.

[7] U.S. Chemical Safety and Hazard Investigation Board, 2023. Storage tank fire at intercontinental terminals company, LLC (ITC) Terminal -investigation report.

[8] Khan F, Reniers G, Cozzani V. Domino effect: its prediction and prevention, methods in chemical process safety, ISBN. Amsterdam: Elsevier; 2021, 9780323915151.

[9] Khan FI, Abbasi S. An assessment of the likelihood of occurrence, and the damage potential of domino effect (chain of accidents) in a typical cluster of industries. J Loss Prev Process Ind 2001;14:283–306. https://doi.org/10.1016/S0950-4230(00)00048-6.

[10] Cozzani V, Reniers G. Dynamic risk assessment and management of domino effects and cascading events in the process industry. Amsterdam: Elsevier; 2021. ISBN: 9780081028384.

[11] Reniers G, Cozzani V. Domino effects in the process industries: modelling, prevention and managing. 2013.

[12] Godoy LA. Buckling of vertical oil storage steel tanks: review of static buckling studies. Thin-Walled Struct 2016;103:1–21. https://doi.org/10.1016/j.tws.2016.01.026.

[13] Godoy LA, Jaca RC, Ameijeiras MP. On buckling of oil storage tanks under nearby explosions and fire. Above ground storage tank oil spills. Elsevier; 2023. p. 199–259. https://doi.org/10.1016/B978-0-323-85728-4.00004-8.

[14] Lees F. Storage. Lees' loss prevention in the process industries. Elsevier; 2012. p. 1889–985. https://doi.org/10.1016/B978-0-12-397189-0.00022-7.

[15] Yang R, Khan F, Neto ET, Rusli R, Ji J. Could pool fire alone cause a domino effect? Reliab Eng Syst Saf 2020;202:106976. https://doi.org/10.1016/j.ress.2020.106976.

[16] Iannaccone T, Scarponi GE, Landucci G, Cozzani V. Numerical simulation of LNG tanks exposed to fire. Process Saf Environ Protect 2021;149:735–49. https://doi.org/10.1016/j.psep.2021.03.027.

[17] Scarponi G, Landucci G, Birk A, Cozzani V. CFD study of the fire response of vessels containing liquefied gases. Chem Eng Trans 2019;77:373–8. https://doi.org/10.3303/CET1977063. SE-Research Articles.

[18] Masum Jujuly M, Rahman A, Ahmed S, Khan F. LNG pool fire simulation for domino effect analysis. Reliab Eng Syst Saf 2015;143:19–29. https://doi.org/10.1016/j.ress.2015.02.010.

[19] Li X, Chen G, Khan F, Lai E, Amyotte P. Analysis of structural response of storage tanks subject to synergistic blast and fire loads. J Loss Prev Process Ind 2022;80:104891. https://doi.org/10.1016/j.jlp.2022.104891.

[20] Wang M, Wang J, Yu X, Zong R. Experimental and numerical study of the thermal response of a diesel fuel tank exposed to fire impingement. Appl Therm Eng 2023;227:120334. https://doi.org/10.1016/j.applthermaleng.2023.120334.

[21] Yang Jianfeng, Zhang B, Chen L, Diao X, Hu Y, Suo G, Li R, Wang Q, Li J, Zhang J, Dou Z. Improved solid radiation model for thermal response in large crude oil tanks. Energy 2023;284:128572. https://doi.org/10.1016/j.energy.2023.128572.

[22] Gubinelli G. Models for the assessment of domino accidents in the process industry. University of Pisa; 2005.

[23] Paltrinieri N, Khan F, Cozzani V. Coupling of advanced techniques for dynamic risk management. J Risk Res 2015;18:910–30. https://doi.org/10.1080/13669877.2014.919515.

[24] Villa V, Paltrinieri N, Khan F, Cozzani V. Towards dynamic risk analysis: a review of the risk assessment approach and its limitations in the chemical process industry. Saf Sci 2016;89:77–93. https://doi.org/10.1016/j.ssci.2016.06.002.

[25] Maidana RG, Parhizkar T, Gomola A, Utne IB, Mosleh A. Supervised dynamic probabilistic risk assessment: review and comparison of methods. Reliab Eng Syst Saf 2023;230:108889. https://doi.org/10.1016/j.ress.2022.108889.

[26] Landucci G, Gubinelli G, Antonioni G, Cozzani V. The assessment of the damage probability of storage tanks in domino events triggered by fire. Accid Anal Prevent 2009;41:1206–15. https://doi.org/10.1016/j.aap.2008.05.006.

[27] Yang Jiahao, Zhang M, Zuo Y, Cui X, Liang C. Improved models of failure time for atmospheric tanks under the coupling effect of multiple pool fires. J Loss Prev Process Ind 2023;81:104957. https://doi.org/10.1016/j.jlp.2022.104957.

[28] Khakzad N, Khan F, Amyotte P, Cozzani V. Risk management of domino effects considering dynamic consequence analysis. Risk Anal 2014;34:1128–38. https://doi.org/10.1111/risa.12158.

[29] Ji J, Tong Q, Khan F, Dadashzadeh M, Abbassi R. Risk-based domino effect analysis for fire and explosion accidents considering uncertainty in processing facilities. Ind Eng Chem Res 2018;57:3990–4006. https://doi.org/10.1021/acs.iecr.8b00103.

[30] Zeng T, Chen G, Yang Y, Chen P, Reniers G. Developing an advanced dynamic risk analysis method for fire-related domino effects. Process Saf Environ Prot 2020;134:149–60. https://doi.org/10.1016/j.psep.2019.11.029.

[31] Su M, Wei L, Zhou S, Yang G, Wang R, Duo Y, Chen S, Sun M, Li J, Kong X. Study on dynamic probability and quantitative risk calculation method of domino accident in pool fire in chemical storage tank area. Int J Environ Res Public Health 2022;19:16483. https://doi.org/10.3390/ijerph192416483.

[32] Zhou J, Reniers G. Dynamic analysis of fire induced domino effects to optimize emergency response policies in the chemical and process industry. J Loss Prev Process Ind 2022;79:104835. https://doi.org/10.1016/j.jlp.2022.104835.

[33] Ricci F, Misuri A, Scarponi GE, Cozzani V, Demichela M. Vulnerability assessment of industrial sites to interface fires and wildfires. Reliab Eng Syst Saf 2024;243:109895. https://doi.org/10.1016/j.ress.2023.109895.

[34] Chen F, Zhang M, Song J, Zheng F. Risk analysis on domino effect caused by pool fire in petroliferous tank farm. Procedia Eng 2018;211:46–54. https://doi.org/10.1016/j.proeng.2017.12.136.
[35] Cui X, Zhang M, Pan W. Dynamic probability analysis on accident chain of atmospheric tank farm based on Bayesian network. Process Saf Environ Protect 2022;158:146–58. https://doi.org/10.1016/j.psep.2021.10.040.
[36] Yang Y, Chen G, Chen P. The probability prediction method of domino effect triggered by lightning in chemical tank farm. Process Saf Environ Protect 2018; 116:106–14. https://doi.org/10.1016/j.psep.2018.01.019.
[37] Landucci G, Argenti F, Tugnoli A, Cozzani V. Quantitative assessment of safety barrier performance in the prevention of domino scenarios triggered by fire. Reliab Eng Syst Saf 2015;143:30–43. https://doi.org/10.1016/j.ress.2015.03.023.
[38] Xu Z, Saleh JH. Machine learning for reliability engineering and safety applications: review of current status and future opportunities. Reliab Eng Syst Saf 2021;211:107530. https://doi.org/10.1016/j.ress.2021.107530.
[39] Abid A, Khan MT, Iqbal J. A review on fault detection and diagnosis techniques: basics and beyond. Artif Intell Rev 2021;54:3639–64. https://doi.org/10.1007/s10462-020-09934-2.
[40] Wang H, Zheng J, Xiang J. Online bearing fault diagnosis using numerical simulation models and machine learning classifications. Reliab Eng Syst Saf 2023; 234:109142. https://doi.org/10.1016/j.ress.2023.109142.
[41] Nassif AB, Talib MA, Nasir Q, Dakalbab FM. Machine learning for anomaly detection: a systematic review. IEEE Access 2021;9:78658–700. https://doi.org/10.1109/ACCESS.2021.3083060.
[42] Zhang C, Hu D, Yang T. Research of artificial intelligence operations for wind turbines considering anomaly detection, root cause analysis, and incremental training. Reliab Eng Syst Saf 2024;241:109634. https://doi.org/10.1016/j.ress.2023.109634.
[43] Huang C, Bu S, Lee HH, Chan KW, Yung WKC. Prognostics and health management for induction machines: a comprehensive review. J Intell Manuf 2023. https://doi.org/10.1007/s10845-023-02103-6.
[44] Xia T, Dong Y, Xiao L, Du S, Pan E, Xi L. Recent advances in prognostics and health management for advanced manufacturing paradigms. Reliab Eng Syst Saf 2018; 178:255–68. https://doi.org/10.1016/j.ress.2018.06.021.
[45] Payette M, Abdul-Nour G. Machine learning applications for reliability engineering: a review. Sustainability 2023;15:6270. https://doi.org/10.3390/su15076270.
[46] Roy A, Chakraborty S. Support vector machine in structural reliability analysis: a review. Reliab Eng Syst Saf 2023;233:109126. https://doi.org/10.1016/j.ress.2023.109126.
[47] Hegde J, Rokseth B. Applications of machine learning methods for engineering risk assessment – a review. Saf Sci 2020;122:104492. https://doi.org/10.1016/j.ssci.2019.09.015.
[48] Bai G, Su Y, Rahman MM, Wang Z. Prognostics of Lithium-Ion batteries using knowledge-constrained machine learning and Kalman filtering. Reliab Eng Syst Saf 2023;231:108944. https://doi.org/10.1016/j.ress.2022.108944.
[49] Li J, Mao W, Yang B, Meng Z, Tong K, Yu S. RUL prediction of rolling bearings across working conditions based on multi-scale convolutional parallel memory domain adaptation network. Reliab Eng Syst Saf 2024;243:109854. https://doi.org/10.1016/j.ress.2023.109854.
[50] Arias Chao M, Kulkarni C, Goebel K, Fink O. Fusing physics-based and deep learning models for prognostics. Reliab Eng Syst Saf 2022;217:107961. https://doi.org/10.1016/j.ress.2021.107961.
[51] Cao L, Zhang H, Meng Z, Wang X. A parallel GRU with dual-stage attention mechanism model integrating uncertainty quantification for probabilistic RUL prediction of wind turbine bearings. Reliab Eng Syst Saf 2023;235:109197. https://doi.org/10.1016/j.ress.2023.109197.
[52] Calzolari G, Liu W. Deep learning to replace, improve, or aid CFD analysis in built environment applications: a review. Build Environ 2021;206:108315. https://doi.org/10.1016/j.buildenv.2021.108315.
[53] Kudela J, Matousek R. Recent advances and applications of surrogate models for finite element method computations: a review. Soft comput 2022;26:13709–33. https://doi.org/10.1007/s00500-022-07362-8.
[54] Li Q, Wang Y, Chen W, Li L, Hao H. Machine learning prediction of BLEVE loading with graph neural networks. Reliab Eng Syst Saf 2024;241:109639. https://doi.org/10.1016/j.ress.2023.109639.
[55] Ye Z, Hsu S-C. Predicting real-time deformation of structure in fire using machine learning with CFD and FEM. Autom Constr 2022;143:104574. https://doi.org/10.1016/j.autcon.2022.104574.
[56] Amin MT, Scarponi GE, Cozzani V, Khan F. Dynamic Domino Effect Assessment (D2EA) in tank farms using a machine learning-based approach. Comput Chem Eng 2024;181:108556. https://doi.org/10.1016/j.compchemeng.2023.108556.
[57] Cozzani V, Gubinelli G, Salzano E. Escalation thresholds in the assessment of domino accidental events. J. Hazard. Mater. 2006;129:1–21. https://doi.org/10.1016/j.jhazmat.2005.08.012.
[58] Amin MT, Scarponi GE, Cozzani V, Khan F. Improved pool fire-initiated domino effect assessment in atmospheric tank farms using structural response. Reliab Eng Syst Saf 2024;242:109751. https://doi.org/10.1016/j.ress.2023.109751.
[59] American Petroleum Institute. API 650 - citeWelded Tanks for oil storage. 2021.
[60] Green DW, Perry RH. Perry's chemical engineers' handbook, eighth edition. 8th ed. New York: McGraw-Hill Education; 2008. /. editorISBN:9780071422949.
[61] Goodfellow IJ, Bengio Y, Courville A. Deep learning. Cambridge, MA, USA: MIT Press; 2016.
[62] Hastie T, Tibshirani R, Friedman J. The elements of statistical learning, springer series in statistics. New York, NY: Springer New York; 2009. https://doi.org/10.1007/978-0-387-84858-7.
[63] Sharma Sagar, Sharma Simone, Athaiya A. Activation functions in neural networks. Towards Data Sci 2017;6:310–6.
[64] Hahn, G.J., 2007. The coefficient of determination exposed !
[65] Yu, T., Zhu, H., 2020. Hyper-parameter optimization: a review of algorithms and applications.
[66] Yang L, Shami A. On hyperparameter optimization of machine learning algorithms: theory and practice. Neurocomputing 2020;415:295–316. https://doi.org/10.1016/j.neucom.2020.07.061.
[67] Liashchynskyi, Petro, Liashchynskyi, Pavlo, 2019. Grid search, random search, genetic algorithm: a big comparison for NAS.
[68] Wolpert DH, Macready WG. No free lunch theorems for optimization. IEEE Trans Evol Comput 1997;1:67–82. https://doi.org/10.1109/4235.585893.
[69] NORSOK. Technical safety - NORSOK S-001:2020+AC. 2020.
[70] Lowesmith BJ, Hankinson G, Acton MR, Chamberlain G. An overview of the nature of hydrocarbon jet fire hazards in the oil and gas industry and a simplified approach to assessing the hazards. Process Saf Environ Protect 2007;85:207–20. https://doi.org/10.1205/psep06038.
[71] Wu Z, Hou L, Wu S, Wu X, Liu F. The time-to-failure assessment of large crude oil storage tank exposed to pool fire. Fire Saf J 2020;117:103192. https://doi.org/10.1016/j.firesaf.2020.103192.
[72] Barber, R.F., Candes, E.J., Ramdas, A., Tibshirani, R.J., 2019. Predictive inference with the jackknife+.
[73] Taquet, V., Blot, V., Morzadec, T., Lacombe, L., Brunel, N., 2022. MAPIE an open-source library for distribution-free uncertainty quantification.
[74] Efron B, Gong G. A leisurely look at the bootstrap, the jackknife, and cross-validation. Am Stat 1983;37:36–48. https://doi.org/10.1080/00031305.1983.10483087.
[75] Zhou J, Reniers G, Cozzani V. Improved probit models to assess equipment failure caused by domino effect accounting for dynamic and synergistic effects of multiple fires. Process Saf Environ Protect 2021;154:306–14. https://doi.org/10.1016/j.psep.2021.08.020.
[76] van den Bosch, C.J.H., Weterings, R.A.P.M., 2005. Heat flux from fires, in: methods for the calculation of physical effects due to releases of Hazardous Materials (Liquids and Gases).
[77] Chen C, Reniers G, Yang M. Dynamic risk assessment of fire-induced domino effects bt - Integrating Safety and security management to protect chemical industrial areas from domino effects. Cham: Springer International Publishing; 2022. p. 49–68. https://doi.org/10.1007/978-3-030-88911-1_2. Chen, C., Reniers, G., Yang, M.